International Journal of Fatigue 81 (2015) 202–212

Contents lists available at ScienceDirect

International Journal of Fatigue

journal homepage: www.elsevier.com/locate/ijfatigue

Estimation of fatigue crack growth behavior for small-sized C-shaped inside edge-notched tension (CIET) specimen using compliance technique

C. Bao *, L.X. Cai, C. Dan

Applied Mechanics and Structure Safety Key Laboratory of Sichuan Province, School of Mechanics and Engineering, Southwest Jiaotong University, Chengdu 610031, People's Republic of China

ARTICLE INFO

Article history:
Received 17 July 2015
Received in revised form 7 August 2015
Accepted 10 August 2015
Available online 17 August 2015

Keywords:
Fatigue crack growth
CIET specimen
Compliance technique
Plasticity-induced crack closure
Finite element analysis

ABSTRACT

Being restricted by the relative larger size requirement, traditional and standard fracture specimens are not applicable for the estimation of fatigue crack growth behavior of some very finite-sized components and precious materials. This study develops a small-sized C-shaped inside edge-notched tension (CIET) specimen which has an advantage of specimen minimization and a wide range of adaptability. A systemic compliance technique for estimating fatigue crack growth behavior of CIET specimen has been successfully constructed and experimentally verified. Groups of fatigue crack propagation rate tests of both CIET specimen and CT specimen for 5083-H112 aluminum alloy were carried out. The resulted $da/dN \sim \Delta K$ curves are heavy affected by specimen configuration and load ratio, and the difference between these $da/dN \sim \Delta K$ curves has been successfully removed by introducing the correction of plasticity-induced crack closure effect. Consequently, the feasibility of CIET specimen for estimating fatigue crack propagation behavior for small-sized components and precious materials has been evidently confirmed.

Crown Copyright © 2015 Published by Elsevier Ltd. All rights reserved.

1. Introduction

The estimation of fatigue crack growth behavior is an essential part of fracture mechanics design approach. According to the principle of linear elastic fracture mechanics (LEFM), the stress intensity factor, K, gives a good indication of the stress environment of crack tip under small scale yielding condition. For a mode I cracked body under cyclic loading, the rate of fatigue crack propagation per cycle, da/dN, is governed by the stress intensity factor range, ΔK, which was first pointed out by Paris [1]. The steady region of the curve of da/dN versus ΔK had been paid the most attention in engineering application, and it could be described by the classic Paris's law [2],

$$da/dN = C(\Delta K)^m \tag{1}$$

where C and m are material constant which should be experimentally measured. The fatigue crack growth curves are typically and experimentally determined by using some standard specimens with through-thickness cracks, such as central cracked tension (CCT) specimen [3], compact tension (CT) specimen [3,4], disk-shaped compact tension (DCT) specimen [4], single edge-notched bending (SENB) specimen [4], single edge-notched tension (SENT) specimen [5,6], double edge-notched tension (DENT) specimen [7], etc. These different specimen configurations should be conditionally chosen to be appropriate for the real structural components in consideration of the dimension and the shape of components.

Taking into account the characteristic of specimen configuration and the corresponding loading fixture, all those standard specimens are not available for the laboratory measurements of fatigue crack growth behavior for some very finite-sized components and precious materials. To satisfy the test requirement of some special components, several nonstandard specimen were adopted. For example, a type of circumferentially cracked round bar was commonly applied to estimate the fracture properties of rod-like materials [8,9], but it still had the specimen length requirement to implement tensile or torsional loading, and was not applicable for metallic plates. Besides, another type of axial cracked pin-loading tension (PLT) specimen was employed to assess the fracture properties of small thin-walled and thick-walled pipes [10–12], this type of specimen was only suitable for small pipes but lack of universality.

All the above-mentioned specimens have their shortcomings in the estimation of fatigue crack growth for small-sized components and precious materials. As is known to all, the mechanical properties of welded component exhibit strong inhomogeneous within the region of weld seam and heat affected zone. The statistic law

* Corresponding author. Tel.: +86 28 87600850; fax: +86 28 87600797.
E-mail addresses: bchxx@163.com (C. Bao), lix_cai@263.net (L.X. Cai).

http://dx.doi.org/10.1016/j.ijfatigue.2015.08.011
0142-1123/Crown Copyright © 2015 Published by Elsevier Ltd. All rights reserved.

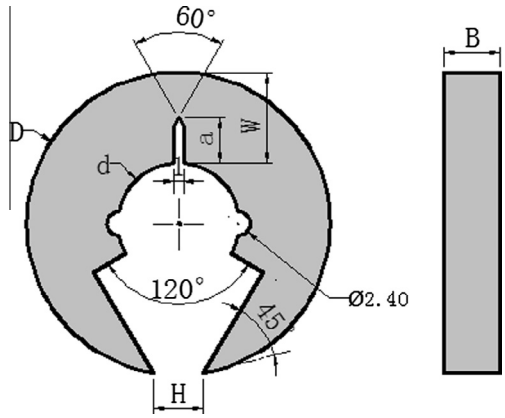

Fig. 1a. The CIET specimen configuration.

Fig. 1b. The real picture of a CIET specimen.

of fatigue crack growth of the welded components may not be discussed further unless obtaining enough samples from the weld zone of interest by using a type of small-enough specimen. In the estimation of fracture properties of irradiated components, the specimen minimization is one of the most concerned factors in view of very high cost.

This study develops a small-sized and wide-adaptive C-shaped inside edge-notched tension (CIET) specimen and its loading fixture. Based on linear elastic finite element analyses, the determination of stress intensity factor and instantaneous crack length measurement by compliance technique have been successfully established. The 5083-H112 aluminum alloy was employed to conduct fatigue crack growth rate tests for both CIET and CT specimens. To eliminate the effect of specimen configuration and load ratio on the fatigue crack propagation law of CIET and CT specimens, a classical plasticity-induced crack closure model has been introduced and discussed in detail.

2. Design of CIET specimen and fixture

2.1. The configuration of CIET specimen

In order to meet the requirements of specimen miniaturization and loading characteristic of mode I crack body, a small-size C-shaped inside edge-notched tension (hereinafter called CIET) specimen is designed by referring to a standard DCT specimen recommended in ASTM E1820-11, as shown in Fig. 1. The CIET specimen is in the shape of C-shaped ring containing an inside single mode I crack. The outer diameter of the ring is defined as D, and the inner diameter is denoted as d. Here, α is defined as the ratio of the inner diameter, d, to the outer diameter, D. This specimen provides a pair of integral knife edges that support the arms of displacement gage, and the space of the two knife edges is variable to match the gage length of displacement measurement, and is denoted as H. Here, the gage length H is 5 mm in this study, which conforms the requirement of a standard crack opening displacement extensometer produced by MTS Systems Corporation. The two ends of the knife edges will be served as the reference points of crack mouth opening displacement of CIET specimen. Additionally, parallel alignment of the knife edges shall be maintained to within 1°. As seen from Fig. 1a, two semicircular holes are symmetrically set normal to the crack face. For the configuration of initial notch, both straight-through slot and chevron notch are allowed. If a chevron form of notch is used, the root radius may be 0.25 mm or less. If a spark-eroded straight-through notch is used, the width may be less than 0.15 mm and the root radius may not be greater than 0.1 mm. The initial crack size a_0 is marked from the intersection point of the notch and inner surface of the ring to the crack tip. The difference between inner and outer radius of the CIET specimen is defined as specimen width, W, and the length perpendicular to the cross section of CIET specimen denotes specimen thickness, B. The inner radius of CIET specimen should match the design of fixture, the outer radius of CIET specimen can be determined according to the practical size of component. Importantly, in the design of the specimen size, the load capacity of the clevis pins must be essentially taken into account and the opening width of the inside circle of CIET specimen should conform the installation of clevis pins. In this study, a typical CIET specimen with inner diameter of 12 mm is fixed, the diameter of the loading semicircular hole is also fixed at 2.4 mm and the thickness B and the ratio of crack size to specimen width a/W are variable. As seen from Fig. 1b, the expected size of a CIET specimen is a little bit larger than a coin of 1 RMB, and it has great advantage of less material consumption and remarkable cost saving. Therefore, the CIET specimen is especially suitable for testing the fracture properties of small-size components and precious materials.

2.2. The fixture of CIET specimen

The fixture suitable for testing CIET specimen is illustrated in Fig. 2. It consists of a fixed clevis and a renewable load transfer mechanism. The diameter of the gripped end of the clevis should conform the requirement of testing machine. The space of the bottom end of the clevis must be large enough to contain the CIET specimen. A tenon and mortise joint is designed to connect the clevis and the load transfer mechanism. To increase the stability of the connection, the two parts are additionally bolted. The load transfer mechanism has a removable pin, and the diameter of the pin is a little bit smaller than that of the loading semicircular hole on the CIET specimen. Both ends of the CIET specimen are held in such a fixture and loaded through pins, in order to allow rotation of the specimen during testing. The pin should be fabricated using steels with sufficient strength to elastically resist indentation by the specimen.

3. Estimation of stress intensity factor, *K*, and instantaneous crack size for CIET specimen

3.1. Finite element model for CIET specimen

To get the relationship between stress intensity factor, K, the specimen geometrical dimensions, and the load and displacement of CIET specimen, detailed linear elastic finite element analyses are performed on plane-stress, plane strain and 3D models for a wide range of CIET specimens, respectively. The analysis matrix includes specimens with $a/W = 0.2$–0.9 with increments of 0.1, and $\alpha = 0.2$–0.6 with increments of 0.1. For the analysis of 3D model, the specimen thickness is set to be 5 mm. These analyses adopt conventional values for the elastic constants, $E = 200$ GPa and $\nu = 0.3$.

The commercial finite element code ANSYS was used to simulate the loading of CIET specimen. Taking into account the symmetry in

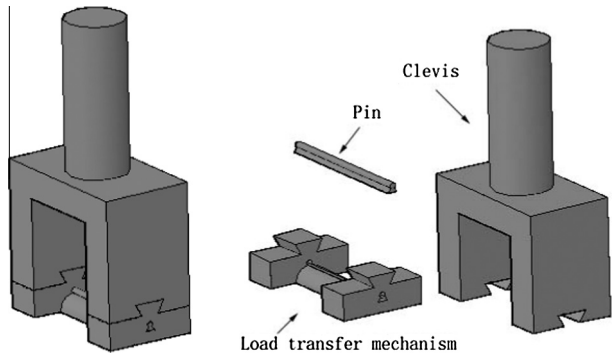

Fig. 2. The configuration of the fixture for CIET specimen.

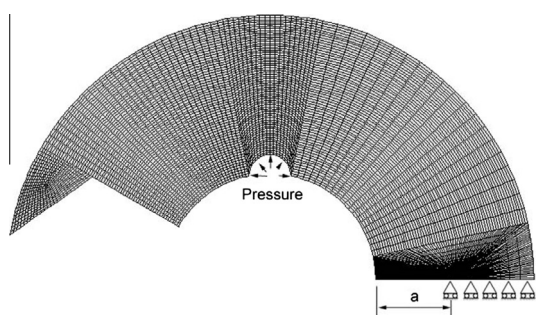

Fig. 3. The 2D finite element model of CIET specimen.

specimen geometry, crack and loading configuration, one-half of the specimen testing setup for 2D model and one-fourth of the specimen testing setup for 3D model are constructed, as shown in Figs. 3 and 4, respectively. The 2D 8-node structural solid element (Plane183) was used for the 2D specimen model under both plane stress and plane strain conditions. The 3D 20-node structural solid element (Solid186) was used for the 3D specimen model. These two types of element satisfy the requirement of singular distribution of stress and deformation around the crack tip. To capture the rapidly varying stress and deformation fields for K calculation, refined meshes in the region around the crack tip were carried out. The minimum size of 2D element is 0.2 mm × 0.2 mm, and the minimum size of 3D element is 0.2 mm × 0.2 mm × 0.2 mm. The mesh of 3D model has 10 variable thickness layers defined over the half-thickness ($B/2$), the thickest layer is defined at $z = 0$ with thinner layers defined near the free surface ($z = B/2$) to accommodate strong z variations in the stress distribution. The half-symmetric 2D model for CIET specimen has 17457 nodes and 17200 elements, and the quarter-symmetric 3D model has 192049 nodes and 172000 elements. The 3D model has the same levels of in-plane mesh refinement around the crack tip as the 2D model.

A y-direction symmetrical restriction is set on the un-cracked ligament of CIET specimen in consideration of the symmetry condition. A uniform pressure is loaded on the semicircular loading hole of the specimen, and the movement of the top point of the semicircular loading hole is restricted in the x-direction as this point is attached to the loading axis of testing machine. For 3D model, a z-direction symmetrical restriction is set on the z-direction symmetrical plane ($z = B/2$) in consideration of the symmetric boundary condition.

3.2. Evaluation of crack length using compliance technique

Compliance technique is the most widely used in the laboratory measurement of instantaneous crack length of fracture specimen during fatigue properties testing [13–15]. Here, the specimen

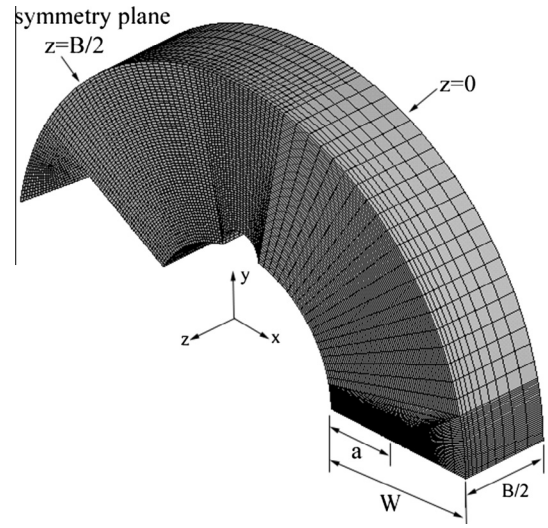

Fig. 4. The 3D finite element model of CIET specimen.

compliance C is defined as the slope of the linear response in terms of crack mouth opening displacement (CMOD) versus load (P) records. The normalized crack length a/W can be related by the specimen compliance C, thickness B, and elastic constant E, via a series of linear elastic finite element analyses for a given specimen geometry with different crack size. In addition, the relationship between normalized crack length a/W and compliance C can also be calibrated experimentally by using plenty of real specimens under linear elastic cyclic loading, but it is much more cost consumption.

To illustrate the compliance technique, Fig. 5 shows the variation of applied load P with increasing CMOD for CIET specimen with the inner to outer diameter ratio $\alpha = 0.4$ and varying crack size as described by a/W ratio, under plane strain condition. For a fixed CMOD, increasing the crack size decreases the specimen stiffness which, consequently, reduces the applied load, P.

By performing a series of finite element analyses for other CIET specimen geometries, the specimen compliance C is processed from P-CMOD records as previously described in Fig. 5. Fig. 6 presents the variation of specimen compliance C with the increase of a/W for the CIET specimen with different α ratios under plane strain condition. To construct a nice describable expression of normalized crack size a/W with respect to compliance C, a normalized compliance u is first defined by,

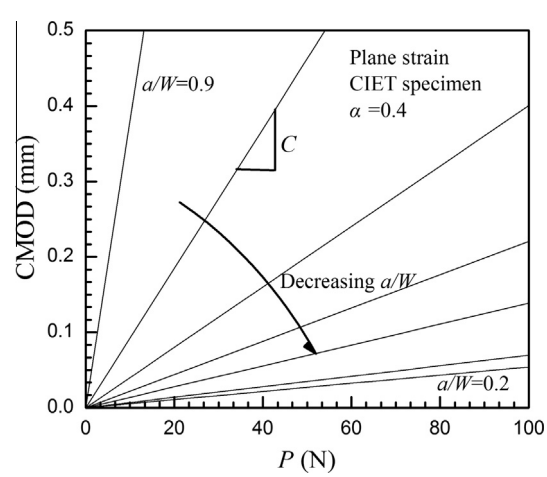

Fig. 5. The P-CMOD curves with different a/W.

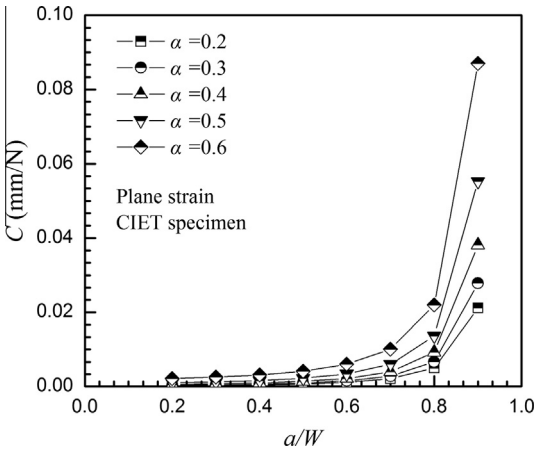

Fig. 6. The relationships between C versus a/W with different α ratios.

$$u = [(B_e EC)^{-0.5} + 1]^{-1} \tag{2}$$

where B_e is the effective thickness of the CIET specimen with side grooves, and is calculated from,

$$B_e = B - \frac{(B - B_N)^2}{B} \tag{3}$$

Here, B_N is the net thickness.

Fig. 7 provides the evolution of crack length to specimen width ratio, a/W, with normalized compliance u for CIET specimen with different inner to outer diameter ratio, α, under plane stress, plane strain and 3D conditions, respectively. The results reveal that the relationships between a/W and u are evidently affected by the inner to outer diameter ratio, α, but are little dependent on the stress status of finite element model. It means that the $a/W \sim u$ relationship with different finite element models for a fixed inner to outer diameter ratio, α, of CIET specimen can be unified, and so it yields,

$$a/W = \frac{d_1 + d_2 u}{1 + d_3 u^{d_4}} \tag{4}$$

Table 1 gives the coefficients of Eq. (4) for the CIET specimen with different inner to outer diameter ratio, α. The analytical result shows that all the predicted errors of Eq. (4) relative to finite element calculation are within 0.5%. The practical and experimental precision of Eq. (4) for the instantaneous crack length estimation of CIET specimen will be discussed below.

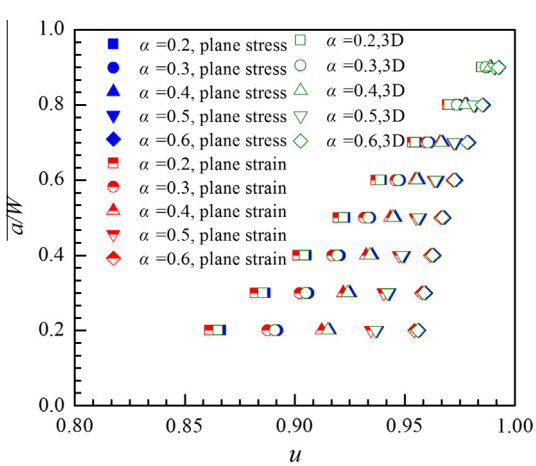

Fig. 7. The relationship between a/W versus normalized compliance u.

Table 1
The coefficients of Eq. (4) for CIET specimen with different α ratios.

α	d_1	d_2	d_3	d_4
0.6	−14.3563	15.1157	−0.2410	−21.2069
0.5	−10.7842	11.6539	−0.1305	−18.7781
0.4	−8.3127	9.2771	−0.0355	−21.2508
0.3	−5.6095	6.5404	−0.0708	10.0316
0.2	−6.3755	7.8471	0.4704	−4.4076

3.3. Evaluation of stress intensity factor K

To obtain the stress intensity factor, K, the analysis is carried out for a prescribed applied load in each specimen within elastic region and the corresponding compliance C are given as described above. There are two different approaches to calculate K. One is a direct method which uses extrapolation technique to calculate K from displacement and stress fields near the crack front. Especially for the commercial finite element code ANSYS, a complete set of procedure using an APDL command "CINT" can implement the K determination based on the extrapolation technique. The other is an indirect method to determine the K from its relation with compliance C and elastic energy release rate G. Based on strain energy principle, strain energy release rate G is a measure of energy available for an increment of area of crack extension, dA, and the specimen with edge crack a can be described as,

$$G = \frac{P^2}{2}\frac{dC}{dA} = \frac{P^2}{2B}\frac{dC}{da} \tag{5}$$

where P is the applied load, B is the thickness of CIET specimen, C is the specimen compliance, and A is the crack area. As is known to all, the strain energy release rate can also be expressed as,

$$G = \frac{K^2}{E'} = \left(\frac{P}{B}\right)^2 \frac{1}{WE'} f^2(a/W) \tag{6}$$

where W is already defined before, E' is the effective elastic modulus ($E' = E$ for plane stress and $E' = E/(1 - \nu^2)$ for plane strain). Combining Eqs. (5) and (6), it gets,

$$f(a/W) = \left[\frac{1}{2} BE' \frac{dC}{d(a/W)}\right]^{1/2} \tag{7}$$

And

$$K = \frac{P}{B\sqrt{W}} f(a/W) \tag{8}$$

By differentiating the nonlinear function derived from $C \sim a/W$ curves as shown in Fig. 6, the $dC/d(a/W)$ as a function of a/W is obtained. Because of the highly nonlinear characteristic of the $C \sim a/W$ curves, these curves are piecewise fitted by using 2-order polynomial function, respectively. Then the curve of $dC/d(a/W)$ versus a/W is again fitted by nonlinear regression analysis to find a suitable function of a/W. Square root of the products of $dC/d(a/W)$, B and E' are evaluated and those values are further re-plotted to obtain $f(a/W)$ as a function of a/W.

According to the first approach, the stress intensity factor K of CIET specimen can also be described by Eq. (8). Fig. 8 gives the geometric function $f(a/W)$ with increasing a/W for CIET specimen with $\alpha = 0.4$ and 0.5 under plane strain condition, obtained from the direct approach 1 and the indirect approach 2, respectively. It is evidently shown that the geometric function $f(a/W)$ determined by the indirect approach is larger than that determined by the direct approach for the both values of α. This is because of the use of piecewise polynomial functions in fitting the $C \sim a/W$ curve and subsequently differentiating to derive the expression of $f(a/W)$ in case of the indirect approach 2, which may not have sufficient

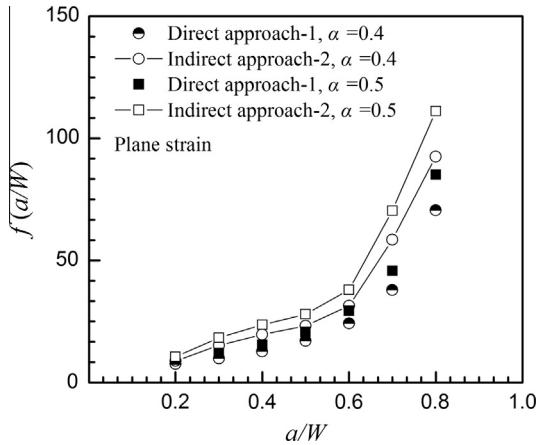

Fig. 8. The comparison of $f(a/W) \sim a/W$ relations resulted from different approaches.

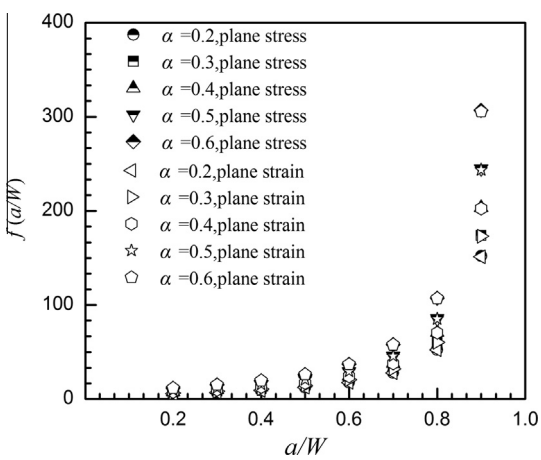

Fig. 9. The relationships between $f(a/W)$ and a/W for CIET specimen under plane stress and plane strain conditions.

precision. Hence, the direct approach 1 seems to be more appropriate for determining the geometric function $f(a/W)$.

Fig. 9 shows the variation of $f(a/W)$ with respect to a/W for CIET specimen with different values of α, under plane stress and plane strain conditions, respectively. It can be noted that $f(a/W)$ is a monotonically function of a/W in the whole range of 0.2–0.8. A very good agreement is observed between plane stress and plane strain solutions for CIET specimen with a fixed value of α. Nevertheless, the ratio α, has remarkable influence on the geometric function $f(a/W)$. Consequently, the derived expression for the geometric function $f(a/W)$ is given as,

$$f(a/W) = c_1(a/W)^{c_2} + c_3(a/W)^{c_4} + c_5 \tag{9}$$

Where the coefficients c_1–c_5 are related by different values of α, as listed in Table 2.

4. Materials and experiment procedure

In this study, two different materials, such as 5083-H112 aluminum alloy and a type of turbine rotor material 26NiCrMoV11-5 were employed to verify the validity of the CIET specimen applied for fatigue crack propagation estimation for small components. The chemical composition of 5083-H112 aluminum alloy is: Si + Fe, 0.45%; Cu, 0.1%; Mn, 0.1%; Mg, 2.2–2.8%; Cr, 0.15–0.35%; Zn, 0.1%; in weight. The chemical composition of 26NiCrMoV11-5 is: C, 0.26–0.32%; Si ⩽ 0.07%; Mn ⩽ 0.4%; Mo, 0.3–0.45%; Cr, 1.4–1.7%; Ni, 2.8–3%; V ⩽ 0.15%; P ⩽ 0.007%; S ⩽ 0.007%; in weight. The conventional mechanical properties of the two materials are listed in Table 3. Both 5083-H112 and 26NiCrMoV11-5 were used to fabricate CIET specimens with different dimensions. Simultaneously, the 5083-H112 aluminum alloy was also used to fabricate traditional CT specimens with different thickness for verifying the validity of CIET specimen.

Table 2
The coefficients of Eq. (9).

Coefficient	$\alpha = 0.6$	$\alpha = 0.5$	$\alpha = 0.4$	$\alpha = 0.3$	$\alpha = 0.2$
c_1	120.3243	827.0858	81.2623	592.2529	519.8693
c_2	2.9995	15.3401	3.0721	15.4641	15.5416
c_3	1032.8602	96.8041	689.9915	70.3016	62.2053
c_4	15.2898	3.0332	15.3975	3.1160	3.1644
c_5	11.4109	9.0479	7.4698	6.3430	5.4997

Table 3
The mechanical properties of test materials.

Material	Young's modulus (MPa)	Yield stress (MPa)	Ultimate strength (MPa)	Elongation after fracture (%)
26NiCrMoV11-5	185,700	790	915	17.6
5083-H112	86,600	141	297	15

The configuration and dimension of CT specimen is shown in Fig. 10. A group of CIET specimens with a fixed thickness of 15 mm and different values of α and a/W ratio were tested under elastic cyclic loading but without crack growth to verify the precision of Eq. (4). The other CIET specimens and all the CT specimens were tested referring to standard fatigue crack growth rate testing procedure. The inner to outer diameter ratio α of these CIET specimens for fatigue crack growth rate tests was 0.4, and the initial crack size to width ratio, a/W, was also fixed at 0.2, but the thickness of these CIET specimens were 5 mm, 7,85 mm and 15 mm, respectively. Similarly, the CT specimens for fatigue crack growth rate tests had fixed width $W = 50$ mm and initial $a/W = 0.2$, but different thickness of 5 mm and 10 mm, respectively. All specimens for the fatigue crack growth rate tests were firstly pre-cracked to get a sharp enough crack, and then were cyclic loaded accompanying with crack growth under different load ratio of $R = 0.1$, 0.3 and 0.5, respectively.

All the tests were conducted on an electromechanical test machine MTS809 with a load frame of 25 kN capacity under tension. A standard crack opening displacement extensometer MTS632.02F-20 was used to measure the CMOD of CIET specimen and CT specimen, whose gage length was 5 mm and had a 4 mm full range of displacement measurements. Fig. 11 shows the actual photograph of fatigue crack growth rate experiments on CIET and CT specimens, respectively.

5. Results and discussion

5.1. The validity of Eq. (4) used for instantaneous crack length determination of CIET specimen

As mentioned above, the CIET specimens by made of 26NiCrMoV11-5 and 5083-H112 with fixed thickness of 15 mm and different crack size and α ratio, were tested to check the precision of Eq. (4). Fig. 12 gives the predicted crack size from Eq. (4), comparing with the real value for each CIET specimen. It can be evidently noted that Eq. (4) has a nice precision for the crack

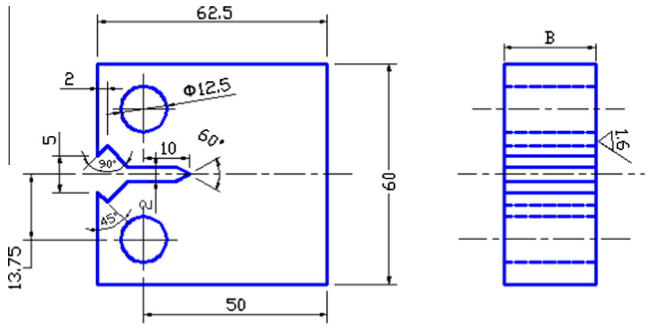

Fig. 10. The configuration and dimension of CT specimen.

size estimation of CIET specimen based on compliance principle, and all the predicted data are within ±5% error scatter band. It can be concluded that Eq. (4) is expectantly appropriate for the on-line monitoring of crack size of CIET specimen during fatigue crack propagation rate test in engineering application.

5.2. The elementary results of fatigue crack growth behavior for CIET and CT specimens

As described before, only 5083-H112 was employed to study the fatigue crack growth rate by using CIET and CT specimens with different thickness, B, and load ratio, R. Fig. 13 gives the relations between fatigue crack growth rate, da/dN, versus the stress intensity factor range, ΔK, obtained from CIET and CT specimens with fixed thickness B and load ratio $R = 0.1$, respectively. Here, the two CIET specimens have the same thickness $B = 15$ mm, and the thickness of the CT specimens is 10 mm. Obviously, for both CIET and CT specimens, the $da/dN \sim \Delta K$ curves of the same two specimens are consistent. It can be concluded that the homogeneity of the used 5083-H112 aluminum alloy has been strongly ensured, so the dispersion of material on the fatigue crack growth of both CIET and CT specimen can be out of consideration. However, the $da/dN \sim \Delta K$ curves of CIET specimens are quite different from those of CT specimens. This will be discussed in detail in the following sections.

Fig. 14 shows the relations between fatigue crack growth rate, da/dN, versus stress intensity factor range, ΔK, obtained from CIET specimens with different thickness $B = 5$ mm, 7.85 mm and 15 mm and load ratio $R = 0.1$, 0.3 and 0.5, respectively. It can be seen that the curves of $da/dN \sim \Delta K$ for CIET specimens with different B

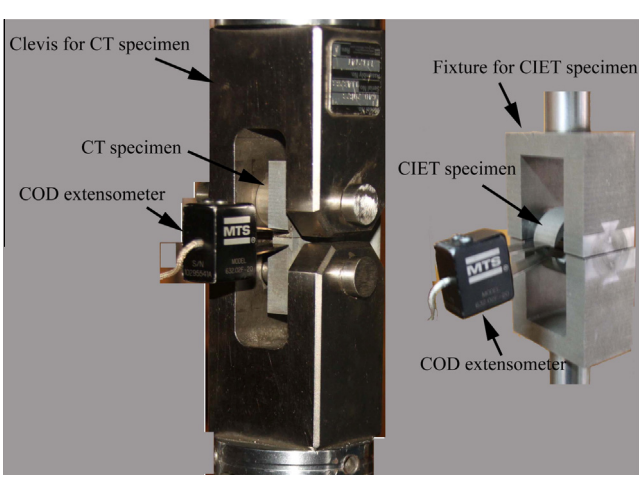

Fig. 11. Actual photograph of fatigue crack growth rate experiments on CT and CIET specimens.

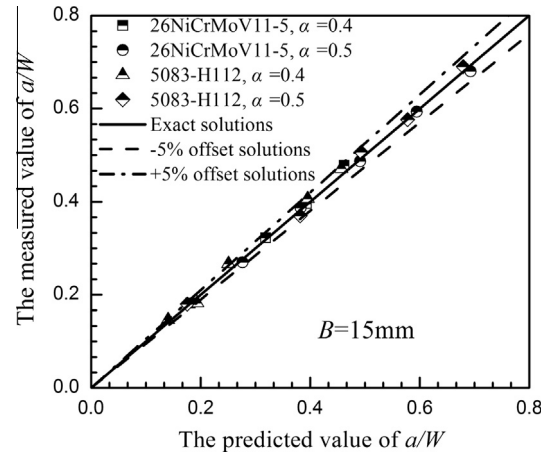

Fig. 12. The validity of Eq. (4) verified by experiments.

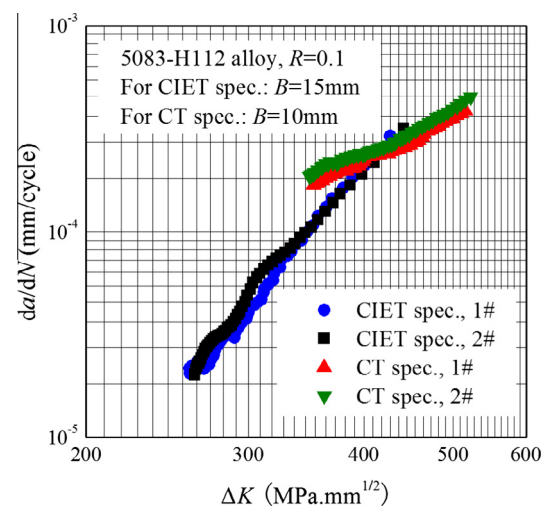

Fig. 13. The repeatability of $da/dN \sim \Delta K$ curves of CIET and CT specimens.

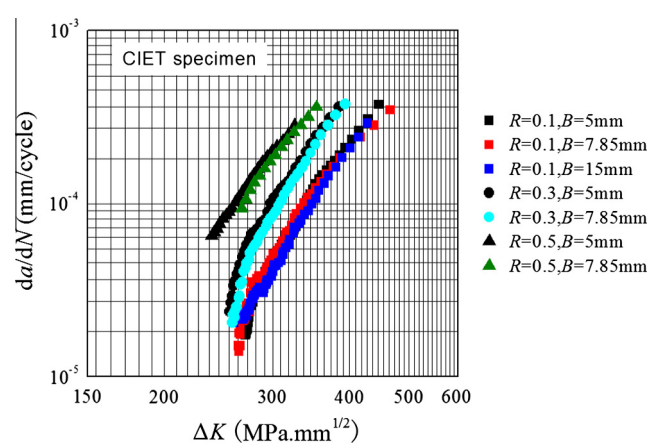

Fig. 14. The relations between da/dN versus ΔK for CIET specimens with different thickness B and load ratio R.

coincide well with each other for each fixed load ratio R, so the influence of the specimen thickness B on the fatigue crack growth behavior of CIET specimen for 5083-H112 aluminum alloy can be evidently neglected. From Fig. 14, it also can be noted that, the load ratio has an obvious effect on the fatigue crack growth behavior of CIET specimen for 5083-H112 alloy under a fixed specimen

thickness. With increase of load ratio, the $da/dN \sim \Delta K$ curve becomes much higher, but the resistance of fatigue crack propagation of CIET specimen suddenly decreases.

Fig. 15 presents the curves of $da/dN \sim \Delta K$ obtained from CT specimens with different thickness $B = 5$ mm, 10 mm and load ratio $R = 0.1$, 0.3 and 0.5, respectively. Being different from CIET specimen, the $da/dN \sim \Delta K$ curves are affected by the specimen thickness for each load ratio, the curve of thinner CT specimen is remarkable higher than that of thicker CT specimen. The load ratio also has notable effect on the fatigue crack growth behavior of CT specimen for 5083-H112 under a fixed specimen thickness. The larger load ratio leads to the weaker resistance of fatigue crack propagation of CT specimen, which is also observed in the fatigue crack growth rate tests of CIET specimen as observed in Fig. 14.

Accordingly, the fatigue crack growth behavior of 5083-H112 is evidently affected by the specimen configuration and load ratio, the $da/dN \sim \Delta K$ curves distribute within a wide region of scatter. It is difficult to assess the fatigue crack growth behavior of materials using CIET specimen if taking no account of the effect of specimen configuration and load ratio.

5.3. The correction of $da/dN \sim \Delta K$ curves in consideration of crack closure

As discussed above, the $da/dN \sim \Delta K$ curves of 5083-H112 aluminum alloy by using CIET and CT specimens are quite different, and these curves present notable effect of specimen thickness and load ratio. Actually, the different properties of fatigue crack growth from different specimen configurations and load ratio may be explained by plasticity-induced crack closure. The plasticity-induced crack closure phenomenon is an intrinsic aspect of the mechanics of growing fatigue cracks, and it was first proposed by Elber [16]. Since then, the plasticity is regarded as the primary mechanism of crack closure under many conditions, even though several additional closure mechanisms have been investigated. During cyclic loading, large tensile strains develop near the crack tip, which are not fully reversed upon unloading as crack growing. It leads to the formation of a plastic wake, with plastic deformation behind the crack tip induced in a direction normal to the advancing crack [17].

For fatigue cracks, there are two types of crack tip plastic zones of interest. One is the forward or monotonic plastic zone, the region of material experiencing plastic deformation when the cracked member is subjected to the maximum load in the cycle. The other is the reversed or cyclic plastic zone, the smaller region of material within the forward zone which undergoes reversed plasticity upon unloading to minimum load. The most widely quoted forward plastic zone size, r_p, is given by [18],

$$r_p = \frac{1}{2\pi}\left(\frac{K_{max}}{\sigma_Y}\right)^2 \tag{10}$$

Here, σ_Y is flow stress. The plasticity-induced crack closure causes a corresponding decrease in the size of the reversed plastic zone, and further leads the decrease in the effective stress intensity factor range. By taking crack closure into account, a simple model for estimating the reversed plastic zone size, Δr_p, was proposed by McClung [18].

$$\frac{\Delta r_p}{r_p} = \left[\frac{U(1-R)}{2-(1-U)(1-R)\frac{\sigma_{max}}{\sigma_Y}}\right]^2 \tag{11}$$

where R is the load ratio and calculated by $\sigma_{min}/\sigma_{max}$, U is the effective stress ratio. The effective stress ratio is directly related by crack closure, so the classic Paris model of the $da/dN \sim \Delta K$ curve under constant amplitude load can be modified,

$$\begin{cases} da/dN = C(\Delta K_{eff})^m = C(U \cdot \Delta K)^m \\ U = \frac{1-\frac{\sigma_{op}}{\sigma_{max}}}{1-R} \end{cases} \tag{12}$$

where ΔK_{eff} is the effective stress intensity factor range, σ_{op} is the opening stress. Many researches have been paid attention to the development of the normalized opening stress σ_{op}/σ_{max} based on theoretical and finite element analyses [19–26]. Here, the model of σ_{op}/σ_{max} proposed by Newman [27,28] is most widely used,

$$\frac{\sigma_{op}}{\sigma_{max}} = \begin{cases} A_0 + A_1R + A_2R^2 + A_3R^3, & \text{for } R \geqslant 0 \\ A_0 + A_1R, & \text{for } -1 \leqslant R \leqslant 0 \end{cases} \tag{13}$$

This equation is valid provided $\sigma_{op}/\sigma_{max} \geqslant R$, and the coefficients A_i are functions of the stress-based constraint factor α_s and σ_{max}/σ_Y,

$$\begin{cases} A_0 = (0.825 - 0.34\alpha_s + 0.05\alpha_s^2)\left[\cos\left(\frac{\pi}{2}\frac{\sigma_{max}}{\sigma_Y}\right)\right]^{1/\alpha} \\ A_1 = (0.415 - 0.071\alpha_s)\frac{\sigma_{max}}{\sigma_Y} \\ A_2 = 2 - 3A_0 - 2A_1 \\ A_3 = 2A_0 + A_1 - 1 \end{cases} \tag{14}$$

The constraint factor α_s is defined as the ratio of the average cohesive stress in the forward plastic zone to the material's yield stress. Newman [29] suggested that the constraint factor α_s may be expressed by a function of the normalized stress intensity factor, $K_{max}/(\sigma_Y B^{0.5})$.

However, Guo et al. [30] revealed that the constraint factor α_s may depend uniquely on the normalized stress intensity factor only when both the crack length and the uncracked ligament size exceed four times the thickness. Further, they rearranged the evolution of the constraint factor α_s in terms of the ratio of the forward plastic zone size to thickness, r_p/B, instead of the normalized stress intensity factor, and then proposed an approximate equation of the relationship between α_s and r_p/B,

$$\alpha_s = \frac{1 + 0.6378[\sqrt{r_p/B} + 2(r_p/B)^2]}{1 - 2\nu + 0.5402[\sqrt{r_p/B} + 2(r_p/B)^2]} \tag{15}$$

where ν is Poisson's ratio. The lower bound for the constraint factor α_s is 1 which represents under plane stress status, and the upper bound for α_s is 3 under plane strain status.

Based on Eq. (15), the constraint factor α_s can be uniquely described by the r_p/B ratio, irrespective of the ratio of crack length to thickness.

It is worthy of noting that Eq. (13) of the normalized opening stress is derived by using CCT specimen in Newman's work, so it

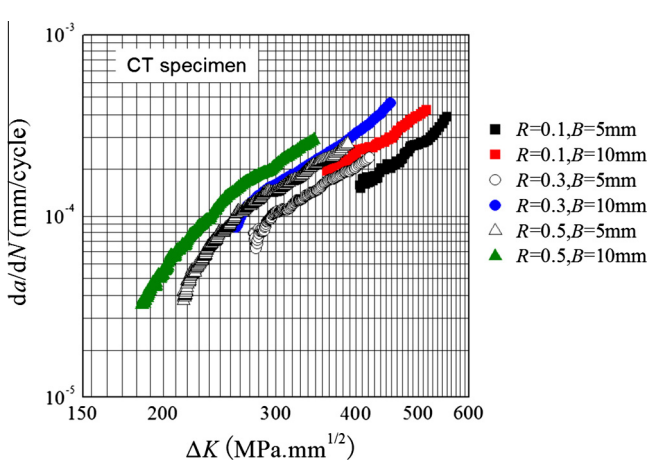

Fig. 15. The relations between da/dN versus ΔK for CT specimen with different thickness B and load ratio R.

needs to be corrected when used to estimate the opening stress for other specimen geometry. Newman [31] has suggested that the opening stress of other specimen configuration can be related to that of CCT specimen by using the results of CCT specimen and defining an equivalent maximum stress $\sigma_{\max,\mathrm{eff}}$ to replace the maximum stress $\sigma_{\max}$ in Eq. (14),

$$\sigma_{\max,eff} = \sigma_{\max}\frac{F_{\mathrm{spec}}}{F_{\mathrm{CCT}}} \tag{16}$$

where F_{spec} and F_{CCT} are the geometry factor of a specified specimen configuration and CCT specimen, respectively. And the geometry factor F can be defined from the expression of stress intensity factor K by McClung [32],

$$K = F\sigma\sqrt{\pi a} \tag{17}$$

For CIET specimen, Eq. (8) has already given the calculation of K for this specimen in laboratory measurement, so by combining Eq. (8) with Eq. (17), the geometry factor F_{CIET} corresponding to CIET specimen can be deduced as,

$$F_{\mathrm{CIET}} = \frac{f(a/W)}{\sqrt{\pi a/W}} \tag{18}$$

For CCT specimen, the engineering measurement of K is recommended in ASTM E647-11 [3],

$$K = \frac{P}{B}\sqrt{\frac{\pi a}{W^2}\sec\left(\frac{\pi a}{W}\right)} \tag{19}$$

Similarly, the expression of K for CT specimen can also be found in ASTM E647-11 [3],

$$\begin{cases} K = \frac{P}{B\sqrt{W}}g(a/W) \\ g(a/W) = \frac{(2+a/W)}{(1-a/W)^{1.5}}[0.886 + 4.64(a/W) \\ \qquad -13.32(a/W)^2 + 14.72(a/W)^3 - 5.6(a/W)^4] \end{cases} \tag{20}$$

Combining Eq. (17) with Eqs. (19) and (20), the geometry factors for CCT and CT specimens can be given, as follows,

$$F_{\mathrm{CCT}} = \sqrt{\frac{\sec\left(\frac{\pi a}{2W}\right)}{2}} \tag{21}$$

$$F_{\mathrm{CT}} = \frac{g(a/W)}{\sqrt{\pi a/W}} \tag{22}$$

Fig. 16 shows the variation of geometry factor F_{spec} with increasing a/W for CCT, CT and CIET specimens, respectively. To be convenient application, the geometry factor of these three specimens can be unified as,

$$F_{\mathrm{spec}} = \frac{k_1 + a/W}{[k_2 + k_3\cdot(a/W)^2]} + k_4 \tag{23}$$

Here, the coefficients k_i are given in Table 4.

For different specimen geometry, the transverse T-stress is another factor which may alter the plastic zone sizes and further affect the crack closure behavior. The T-stress is the second non-singular term in Williams's expression of the elastic stress field at the crack tip, is defined as,

$$\sigma_{ij} = \frac{K_I}{\sqrt{2\pi r}}f_{ij}(\theta) + T\delta_{xi}\delta_{xj} \tag{24}$$

where K_{I} is the mode I stress intensity factor, $f_{ij}(\theta)$ is the non-dimensional angular function, and δ_{ij} is the Kronecker delta. The T-stress is independent of r and acts in a direction parallel to the plane of crack and approximately constant over the crack tip region. It is commonly expressed by a biaxiality ratio β, and can be

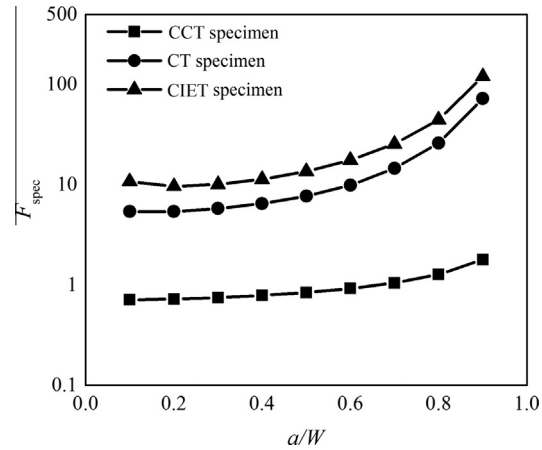

Fig. 16. The relations of F_{spec} versus a/W.

Table 4
The coefficients k_i of Eq. (23).

Coefficients	CCT	CT	CIET
k_1	5.3904	−2.5583	−2.1986
k_2	15.4251	−0.1562	−0.0671
k_3	−13.6389	0.1681	0.0715
k_4	0.3504	−10.3768	−21.0966

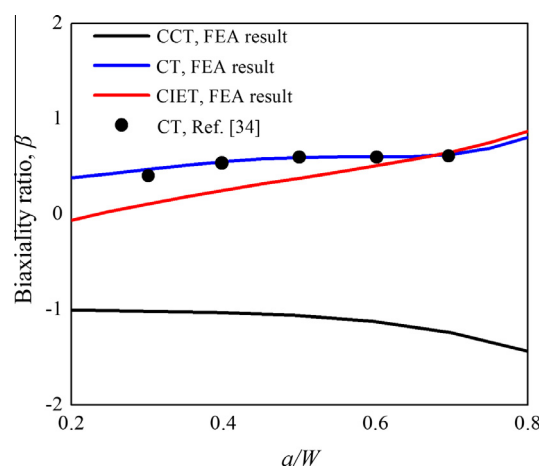

Fig. 17. The evolution of biaxiality ratio β for different specimen geometry.

conveniently determined by stress difference method [33] through finite element analyses (FEA).

$$\beta = \frac{T\sqrt{\pi a}}{K_{\mathrm{I}}} \tag{25}$$

Fig. 17 gives the variation of the biaxiality ratio β with increasing a/W for three different specimen geometry. To check the reasonability of the FEA results, the results of β for CT specimen obtained from Ref. [34] are comparably shown in this figure. It can be seen that the FEA results for CT specimen are in agreement with the results from literature. From Fig. 17, the T-stress of CCT specimen is negative while the T-stress of CT and CIET specimens are mainly positive. The T-stress of CT specimen is slightly larger than that of CIET specimen when $a/W < 0.7$, then the difference diminishes after $a/W > 0.7$. The work of Knésl [35] showed that the lager T-stress would cause smaller plastic zone size. To account

for the effect of T-stress on the reversed plastic zone size and crack closure, Eqs. (11) and (13) should be modified by the replacement flow stress σ_Y with a new effective flow stress σ'_Y [22],

$$\sigma'_Y = \frac{1}{2}\left(T + \sqrt{4\sigma_Y^2 - 3T^2}\right) \tag{26}$$

By comparing Eq. (17) with Eq. (25), the T-stress can be easy determined by the product $\beta F\sigma$.

Fig. 18 shows the evolution of normalized reversed plastic zone size, $\Delta r_p/r_p$, with the increase of σ_{max}/σ_Y, for CT and CIET specimen, respectively. Fig. 19 gives the variation of the corresponding effective stress ratio, U. Because the constraint factor α_s for both CT and CIET specimens for the used 5083-H112 alloy are between 1.8 and 2.1, so only the values of $\Delta r_p/r_p$ and U when $\alpha_s = 2$ are illustrated in these figures. The results indicate that, the difference of $\Delta r_p/r_p$ caused by the T-stress becomes larger when $\sigma_{max}/\sigma_Y > 0.4$ and $a_0/W = 0.2$, and the value of $\Delta r_p/r_p$ for CIET specimen is larger than that of CT specimen because of the less values of T-stress the CIET specimen has. With increasing the load ratio R and a_0/W, the difference becomes less and less, and vanishes especially when $a_0/W = 0.6$. In view of the difference of the normalized reversed plastic zone size, $\Delta r_p/r_p$, the difference of the effective stress ratio, U, consequently exhibits between the two specimens. The less reversed plastic zone size causes the smaller effective stress ratio but stronger effect of crack closure. With the increase of load ratio, R, the effect of crack closure becomes more slightly. On the other hand, with the constraint factor α_s increases, the stress state is closer to plane strain, the crack closure gradually disappears, and this observation agrees well with the findings of Ref. [36] where it reported that the crack closure did not occur under steady-state plane strain conditions.

As discussed above, the experimental curves of da/dN versus ΔK of CIET and CT specimens for 5083-H112 aluminum alloy can be corrected on the basis of the above-modified plastic-induced crack closure model considering the effect of specimen geometry. Fig. 20 shows the corrected $da/dN \sim \Delta K_{eff}$ curves of CIET specimens with different load ratio and specimen thickness. Fig. 21 shows the corrected $da/dN \sim \Delta K_{eff}$ curves of CT specimens with different load ratio and specimen thickness. By comparing with the original results as shown in Fig. 14, the corrected $da/dN \sim \Delta K_{eff}$ curves of CIET specimens with different load ratio and specimen thickness are in good agreement with each other, so the effect of load ratio on the fatigue crack growth behavior of CIET specimen has been evidently eliminated. Similarly, the corrected $da/dN \sim \Delta K_{eff}$ curves of CT specimens with different load ratio and specimen thickness

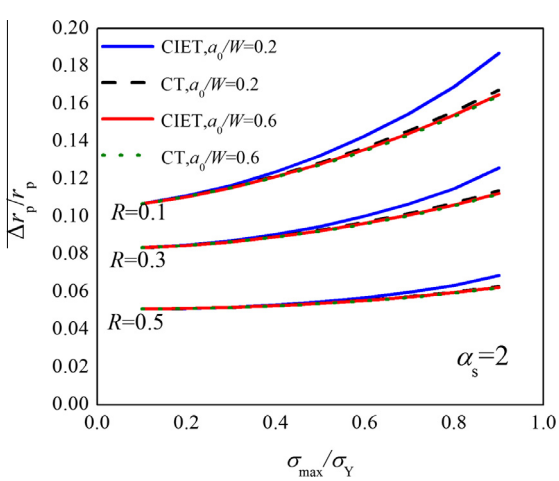

Fig. 18. The evolution of $\Delta r_p/r_p$ with the change of σ_{max}/σ_Y when $\alpha_s = 2$.

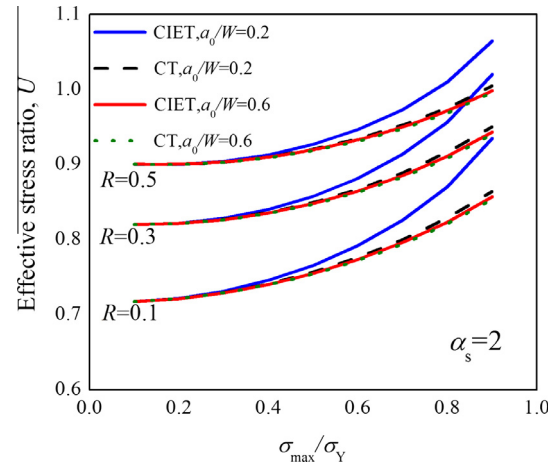

Fig. 19. The evolution of U with the change of σ_{max}/σ_Y when $\alpha_s = 2$.

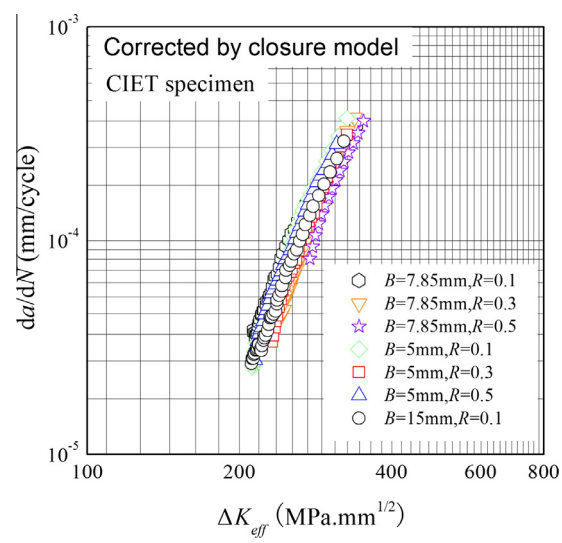

Fig. 20. The corrected $da/dN \sim \Delta K_{eff}$ curves of CIET specimens with different R and B.

are also consistent, and the influence of load ratio and thickness on the fatigue crack growth curves of CT specimen is removed.

Fig. 22 presents the corrected $da/dN \sim \Delta K_{eff}$ curves of both CIET and CT specimens with different load ratio and specimen thickness. It can be noted that all the corrected $da/dN \sim \Delta K_{eff}$ curves distribute within a narrow region of scatter in comparison with the uncorrected results. The lower and upper bounds of the $da/dN \sim \Delta K_{eff}$ curves for 5083-H112 aluminum alloy can be described as,

The lower bound:

$$da/dN = 2.115 \times 10^{-19} \Delta K_{eff}^{6.018} \tag{27}$$

The upper bound:

$$da/dN = 8.522 \times 10^{-18} \Delta K_{eff}^{5.613} \tag{28}$$

It is absolutely concluded that the plasticity-induced crack closure correction can actively remove not only the effect of load ratio and specimen thickness but also the effect of specimen configuration on the fatigue crack growth behavior of 5083-H112 aluminum alloy. The used 5083-H112 alloy is a typical low strain hardening material. The work of McClung [18] indicated that the

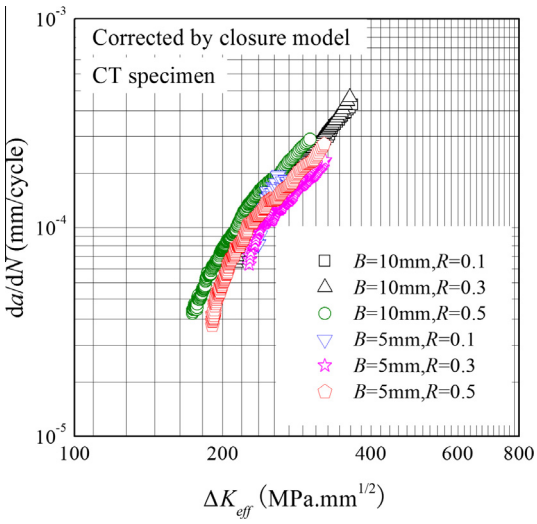

Fig. 21. The corrected $da/dN \sim \Delta K_{eff}$ curves of CT specimens with different R and B.

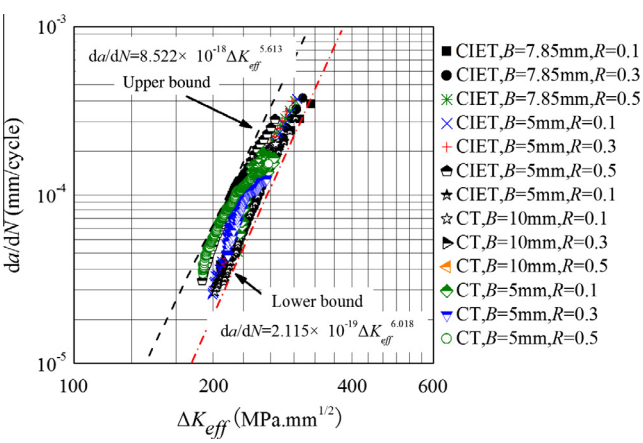

Fig. 22. The corrected $da/dN \sim \Delta K_{eff}$ curves of both CIET and CT specimens with different load ratio and specimen thickness.

crack closure effect on the low strain hardening materials is only slightly stronger than high strain hardening materials. Besides, Parry [38] suggested that strain hardening effect is not a primary factor in crack closure. Therefore, the CIET specimen is appropriate for estimating fatigue crack growth behavior of metals and has a distinct advantage of specimen miniaturization and less cost consumption. Furthermore, the fatigue crack growth curve estimated from the CIET specimen may be coincident with the results from other traditional and standard specimens by introducing the correction of plasticity-induced crack closure.

6. Conclusions

To meet the needs of fatigue crack growth behavior estimation for finite-sized structures and precious materials, a type of small size CIET specimen and the corresponding test method for fatigue crack growth rate based on compliance technique has been proposed. This CIET specimen has an outstanding advantage of less size requirement and cost consumption. According to linear elastic finite element analyses, the high-precision expressions of stress intensity factor and instantaneous crack length measurements of CIET specimen have been established. A series of fatigue crack growth rate experiments on both CIET and CT specimens of 5083-H112 aluminum alloy were conducted to verify the feasibility of using CIET specimen to assess fatigue crack growth behavior of metals. The specimen thickness and the load ratio show strong effects on the $da/dN \sim \Delta K$ curves of CIET specimen, and the curves obtained by CIET specimen are apparently different from those by CT specimen. The effects of specimen configuration and load ratio are mainly resulted from the crack closure effect during the unloading procedure in the fatigue crack growth rate tests. An improved plastic-induced crack closure model has been introduced to correct the $da/dN \sim \Delta K$ curves of both CIET and CT specimens with different thickness and load ratio. The discussions of the effect of T-stress for different specimen geometry on the reversed plastic zone size and the effect stress ratio show that, the CIET specimen gets the slightly larger reversed plastic zone size and thereby leads to less sensitive to crack closure in comparison with CT specimen. The load ratio and the crack tip stress state rather than the strain hardening levels have outstanding influence on the crack closure behavior. When the load ratio is large enough or the crack tip stress state approaches to plane strain, the crack closure effect may vanish. Finally, all the corrected $da/dN \sim \Delta K$ curves are consequently consistent and the Paris law of 5083-H112 aluminum alloy is given.

Acknowledgements

This work was financially supported by the National Natural Science Foundation of China (Grant No. are 11202174 and 11472228). The authors thank the helpful comments and suggestions from anonymous reviewers.

References

[1] Paris PC. The growth of fatigue cracks due to variations in load. Ph.D. thesis. Lehigh University; 1962.
[2] Paris PC, Erdogan F. A critical analysis of crack propagation laws. Trans J Basic Eng 1963;85:528–34.
[3] ASTM E647-11. Standard test method for measurement of fatigue crack growth rates. Annual Book of ASTM Standards. West Conshohocken, PA: American Society for Testing and Materials; 2011.
[4] ASTM E1820-13. Standard test methods for measurement of fracture toughness. Annual Book of ASTM Standards, vol. 3.01. Philadelphia, PA: American Society for Testing and Materials; 2013.
[5] Benachour M, Benguediab M, Hadjoui A. Residual stress effect on fatigue crack growth of SENT specimen. Damage Fract Mech 2009:367–73.
[6] Sultan Amir, Pasha Riffat Asim, Ali Mifrah, et al. Numerical simulation and experimental verification of CMOD in SENT specimen: application on FCGR of welded tool steel. Acta Metall Sin (Engl Lett) 2013;26(1):92–6.
[7] Narasimhachary SB, Saxena A, Newman Jr JC. A double edge notch specimen design for tension-compression fatigue crack growth testing. Eng Fract Mech 2012;92:26–136.
[8] Chen YZ. Stress intensity factors in a finite length cylinder with a circumferential crack. Int J Press Ves Pip 2000;77:439–44.
[9] Berto F, Elices M, Lazzarin P, Zappalorto M. Fracture behavior of notched round bars made of PMMA subjected to torsion at room temperature. Eng Fract Mech 2012;90:143–60.
[10] Samal MK, Sanyal G. A load-separation technique to evaluate crack growth and fracture resistance behavior of thin-walled axially cracked tubular specimens. J Mech Eng Sci 2012;226(6):1447–61.
[11] Samal MK, Sanyal G. An experimental and numerical study of the fracture behavior of tubular specimens in a pin-loading-tension set-up. J Mech Eng Sci 2010;224(1):1–12.
[12] Bertsch J, Hoffelner W. Crack resistance curves determination of tube cladding material. J Nucl Mater 2006;352:116–25.
[13] Ashok Saxena, Hudak Jr SJ. Review and extension of compliance information for common crack growth specimens. Int J Fract 1978;14(5):453–68.
[14] Voss B. On the problem of negative crack growth and load relaxation in single specimen partial unloading compliance tests. CSNI workshop on ductile fracture test methods, Paris; 1983. p. 210–19
[15] Gordon JR. The Welding Institute procedure for an assessment of the accuracy of the unloading compliance method for measuring crack growth resistance curves. Report no. 325/1986; 1986.
[16] Elber W. Fatigue crack closure under cyclic tension. Eng Fract Mech 1970;2:37–45.
[17] Solanki Kiran, Daniewicz SR, Newman Jr JC. Finite element modeling of plasticity-induced crack closure with emphasis on geometry and mesh refinement effects. Eng Fract Mech 2003;70:1475–89.
[18] McClung RC. Crack closure and plastic zone sizes in fatigue. Fatigue Fract Eng Mater Struct 1991;14(4):455–68.

[19] Shercliff HR, Fleck NA. Effect of specimen geometry on fatigue crack growth in plane strain-I. Constant amplitude response. Fatigue Fract Eng Mater Struct 1990;13(3):287–96.
[20] Shercliff HR, Fleck NA. Effect of specimen geometry on fatigue crack growth in plane strain-II. Overload response. Fatigue Fract Eng Mater Struct 1990;13(3):297–310.
[21] Chang T, Guo W. A model for the through-thickness fatigue crack closure. Eng Fract Mech 1999;64:59–65.
[22] Kim JH, Lee SB. Fatigue crack opening stress based on the strip-yield model. Theor Appl Fract Mech 2000;34:73–84.
[23] Meggiolaro Marco Antonio, De Castro Jaime Tupiassu Pinho. On the dominant role of crack closure on fatigue crack growth model. Int J Fatigue 2003;25:843–54.
[24] Savaidis G, Savaidis A, Zerres P, Vormwald M. Mode I fatigue crack growth at notches considering crack closure. Int J Fatigue 2010;32:1543–58.
[25] Varfolomeev I, Luke M, Burdack M. Effect of specimen geometry on fatigue crack growth rates for the railway axle material EA4T. Eng Fract Mech 2011;78:742–53.
[26] Singh Konjengbam Darunkumar, Parry Matthew Roger, Sinclair Ian. A short summary on finite element modelling of fatigue crack closure. J Mech Sci Technol 2011;25(12):3015–24.
[27] Newman Jr JC. A crack-closure model for predicting fatigue-crack growth under aircraft spectrum loading. NASA Technical Memorandum 81941; 1981.
[28] Newman Jr JC. A crack opening stress equation for fatigue crack growth. Int J Fract 1984;24:R131–5.
[29] Newman Jr JC, Crew Jr JH, Biglew CA, Dawicke DS. Variations of a global constraint factor in cracked bodies under tension and bending loading. In: Kirk M, Bakker A, editors. Constraint effects in fracture theory and applications: second volume, ASTM STP 1244. Philadelphia: American Society for Testing and Materials; 1995
[30] Guo W, Wang CH, Rose LRF. The influence of cross-sectional thickness on fatigue crack growth. Fatigue Fract Eng Mater Struct 1999;22(5):437–44.
[31] Newman Jr JC. FASTRAN-II: a fatigue crack growth structural analysis program [R]. NASA TM-104159; 1992.
[32] McClung RC. Finite element analysis of specimen geometry effects on fatigue crack closure. Fatigue Fract Eng Mater Struct 1994;17(8):861–72.
[33] Yang B, Ravi-Chandar. Evaluation of elastic T-stress by the stress difference method. Eng Fract Mech 1999;64:589–605.
[34] Sherry AH, France CC, Goldthorpe MR. Compendium of T-stress solutions for two and three dimensional cracked geometries. Fatigue Fract Eng Mater Struct 1995;18(1):141–55.
[35] Knésl Z, Seitl S, Hutař P. Accounting for effects of constraint on propagation of a fatigue crack. Int Conf Damage Fract Mech 2002:245–53.
[36] Fleck NA. Finite element analysis of plasticity-induced crack closure under plane strain conditions. Eng Fract Mech 1986;25:441–9.